Chinese Journal of Physics 73 (2021) 13–23

Contents lists available at ScienceDirect

Chinese Journal of Physics

journal homepage: www.elsevier.com/locate/cjph

NRQCD analysis of charmonium production with pion and proton beams at fixed-target energies

Chia-Yu Hsieh [a,b,1], Yu-Shiang Lian [a,c,1], Wen-Chen Chang [a,*], Jen-Chieh Peng [d], Stephane Platchkov [e], Takahiro Sawada [f]

[a] Institute of Physics, Academia Sinica, Taipei 11529, Taiwan
[b] Department of Physics, National Central University, 300 Jhongda Road, Jhongli 32001, Taiwan
[c] Department of Physics, National Kaohsiung Normal University, Kaohsiung County 824, Taiwan
[d] Department of Physics, University of Illinois at Urbana-Champaign, Urbana, Illinois 61801, USA
[e] IRFU, CEA, Université Paris-Saclay, 91191 Gif-sur-Yvette, France
[f] Department of Physics, Osaka City University, Osaka 558-8585, Japan

ARTICLE INFO

Keywords:
Charmonium production
Pion PDFs
NRQCD
Color-octet matrix elements
Gluon

ABSTRACT

We present an analysis of hadroproduction of J/ψ and $\psi(2S)$ at fixed-target energies in the framework of non-relativistic QCD (NRQCD). Using both pion- and proton-induced data, a new determination of the color-octet long-distance matrix elements (LDMEs) is obtained. Compared with previous results, the contributions from the $q\bar{q}$ and color-octet processes are significantly enhanced, especially at lower energies. A good agreement between the pion-induced J/ψ production data and NRQCD calculations using the newly obtained LDMEs is achieved. We find that the pion-induced charmonium production data are sensitive to the gluon density of pions, and favor pion PDFs with relatively large gluon contents at large x.

1. Introduction

Since the discovery of the J/ψ resonance in 1974, the study of $c\bar{c}$ and $b\bar{b}$ quarkonium states has significantly improved our understanding of the strong interaction [1–5]. Production of heavy-quark bound states offers important testing grounds for both perturbative and nonperturbative aspects of QCD. From the experimental perspective, quarkonia are readily detected through their dilepton decay, and the associated production cross sections are large compared to other hard processes. Since hadroproduction of quarkonium receives important contribution from gluon–gluon fusion it could serve as a tool for accessing the gluon distributions of interacting hadrons, and particularly for the unstable pion. Our current knowledge on the pion parton distribution functions (PDFs) mainly comes from pion-induced Drell–Yan data. As the Drell–Yan cross sections are dominated by $\bar{q}$-q annihilation, they essentially probe the valence quark distribution in the pion, but leave the sea and the gluon distributions unconstrained. The mounting interest in the pion PDFs is reflected in many publications in the past few years. The pion PDFs were extracted using new and refined global analyses [6–8], or calculated from new theoretical developments, such as the continuum Dyson–Schwinger Equations [9,10], light-front holographic QCD [11], and light-front Hamiltonian [12]. First lattice QCD results on the x-dependence of pion valence structure are also becoming available [13–18].

A significant amount of pion-induced charmonium data has been collected in the past. Recently, we investigated the sensitivity of the fixed-target J/ψ production data to the pion PDFs [19]. The pion-induced J/ψ data on hydrogen and several light-mass

* Corresponding author.
E-mail address: changwc@phys.sinica.edu.tw (W.-C. Chang).
[1] These authors contributed equally to this work.

https://doi.org/10.1016/j.cjph.2021.06.001
Received 25 April 2021; Received in revised form 24 May 2021; Accepted 2 June 2021
Available online 11 June 2021

nuclear targets were compared to next-to-leading-order (NLO) Color Evaporation Model (CEM) [20] calculations using the available global-fit parametrizations of the pion PDFs. Over the energy range considered, the calculations with pion PDFs determined by SMRS [21], GRV [22], JAM [6] and xFitter [7], are all in reasonable agreement with the total cross sections data. In contrast, for the longitudinal momentum x_F distributions, we found that the agreement between data and calculations strongly depends on the magnitude and shape of the gluon distribution in the pion. The data favor pion PDFs with larger gluon strength at large x.

To examine a possible model dependence of our previous observations [19], we extend our work to a more elaborate formalism for quarkonia production, namely, the non-relativistic QCD (NRQCD) [23] approach. This approach is based on a factorization of the heavy-quark pair $Q\bar{Q}$ production and its subsequent hadronization. The production of the $Q\bar{Q}$ pair proceeds through a short-distance partonic interaction, calculated using perturbative QCD. The probability of hadronization of a $Q\bar{Q}$ pair into some quarkonium bound state depends on its spin, color and angular momentum. Being of a non-perturbative nature, the hadronization is described by the associated long-distance matrix elements (LDMEs). The LDMEs, assumed to be universal, are extracted from the experimental data. The values for the color-singlet (CS) LDMEs can be obtained from the decay widths of charmonia or model calculations, while the color-octet (CO) ones are determined from fits to data of transverse-momentum (p_T) differential cross sections, polarization, and p_T-integrated cross sections of charmonium production.

The NRQCD approach is based on the assumption that the factorization holds [23]. However, for low p_T additional effects might have large contributions. Analysis of fixed-target data could provide hints for such effects by assessing the universality of the LDMEs. Such study, focusing exclusively on charmonium hadroproduction from fixed-target experiments, was reported by Beneke and Rothstein [24]. The calculation was performed at partial next-to-leading order (up to $\mathcal{O}(\alpha_s^3)$). Some LDMEs were taken from fits to collider data of p_T-differential cross sections [25,26] while others were fitted to the proton-induced cross section. The resulting LDMEs were used to calculate the pion-induced total cross sections. The calculation was found to lie systematically below the data, for both J/ψ and $\psi(2S)$ production. The failure in describing the pion-induced data was speculated to be due to either inaccurate gluon distributions of pion PDFs or a difference in the higher twist effects between the proton and the pion data [24].

More recently, Maltoni et al. [27] re-analyzed the data of J/ψ and $\psi(2S)$ fixed-target proton-induced cross sections. The pion-induced data were not included in the analysis. Their NRQCD calculation was performed at NLO using the formalism described in Ref. [28]. The initial CO parameters were taken from the Tevatron data [29,30], but the S-wave CO LDMEs for J/ψ and $\psi(2S)$ were allowed to vary. A good description of the data was achieved, at the expense of a strong reduction of the color-octet LDMEs by a factor of 5 to 10, depending on the proton PDFs used.

By using the NRQCD formalism in the fixed-target domain, the primary motivation of our present work is twofold. First, we aim at the determination of a new set of LDMEs that can reproduce both pion and proton-induced J/ψ production cross sections. As the pion contains a valence antiquark, the J/ψ cross section for a pion beam has a larger $q\bar{q}$ contribution than that for a proton beam. Thereby, the pion-induced data provide a stronger constraint on the LDMEs that are responsible for the $q\bar{q}$ part of the cross section. Second, we use this new set of LDMEs to explore the sensitivity of the pion-induced charmonium data to the parametrizations of the pion PDFs. The most recent global fits [6,7] lead to pion gluon distributions which significantly differ from the older pion PDF determinations [21,22], at large and medium parton momenta [19]. According to our previous results [19], these new sets of pion PDFs bring worse agreement between the CEM calculations and the data. It is important to validate these observations with a NRQCD calculation.

To perform this study, we adopt the NRQCD framework explicitly formulated in Ref. [24]. We start with a comparison of NRQCD calculations with the total cross section data for J/ψ and $\psi(2S)$ productions with proton and pion beams. We then vary the CO LDMEs for J/ψ and $\psi(2S)$ production to achieve a consistent description of both proton and pion data. In addition, we use the new LDMEs to explore the sensitivity of the pion-induced J/ψ data to the gluon distribution in the pion. This paper is organized as follows. In Section 2, we introduce the NRQCD framework for the calculations of charmonia cross sections in hadroproduction. A new fit to the fixed-target J/ψ and $\psi(2S)$ production data to determine a new set of LDMEs is presented in Section 3. We further discuss several findings from the present study in Section 4, followed by a summary in Section 5.

2. Charmonium production and NRQCD

In NRQCD, the differential cross section as a function of Feynman x (x_F), $d\sigma/dx_F$ for a charmonium state H ($H = J/\psi$, $\psi(2S)$, or χ_{cJ}) from the hN, ($h = p$, $\bar{p}$, or π) collisions, where h is the beam hadron and N the target nucleon, is [31]

$$\frac{d\sigma^H}{dx_F} = \sum_{i,j=q,\bar{q},G} \int_0^1 dx_1 dx_2 \delta(x_F - x_1 + x_2)$$
$$\times f_i^h(x_1,\mu_F) f_j^N(x_2,\mu_F) \hat{\sigma}[ij \to H](x_1 P_h, x_2 P_N, \mu_F, \mu_R, m_c), \quad (1)$$
$$\hat{\sigma}[ij \to H] = \sum_n C_{c\bar{c}[n]}^{ij}(x_1 P_h, x_2 P_N, \mu_F, \mu_R, m_c) \times \langle \mathcal{O}_n^H[^{2S+1}L_J] \rangle \quad (2)$$

$$x_F = 2p_L/\sqrt{s},\ x_{1,2} = \frac{\sqrt{x_F^2 + 4M_{c\bar{c}}{}^2/s} \pm x_F}{2} \quad (3)$$

where i and j label the type of interacting partons (gluons, quarks and antiquarks), and the $c\bar{c}$ pair is denoted by its color (n), spin (S), orbital angular momentum (L) and total angular momentum (J). Here m_c and $M_{c\bar{c}}$ are the charm quark and $c\bar{c}$ pair masses, f^h and f^N are the incoming hadron and the target nucleon parton distribution functions, evaluated at their respective Bjorken-x values,

Table 1
Relationship of LDMEs and the associated orders of α_s to the scattering processes for various charmonium states in the NRQCD framework of Ref. [24].

H	$q\bar{q}$	GG	qG
J/ψ, $\psi(2S)$	$\langle\mathcal{O}_8^H[^3S_1]\rangle$ $(\mathcal{O}(\alpha_s^2))$	Δ_8^H [a] $(\mathcal{O}(\alpha_s^2))$	
		$\langle\mathcal{O}_1^H[^3S_1]\rangle$ $(\mathcal{O}(\alpha_s^3))$	
χ_{c0}	$\langle\mathcal{O}_8^H[^3S_1]\rangle$ $(\mathcal{O}(\alpha_s^2))$	$\langle\mathcal{O}_1^H[^3P_0]\rangle$ $(\mathcal{O}(\alpha_s^2))$	
χ_{c1}	$\langle\mathcal{O}_8^H[^3S_1]\rangle$ $(\mathcal{O}(\alpha_s^2))$	$\langle\mathcal{O}_1^H[^3P_1]\rangle$ $(\mathcal{O}(\alpha_s^3))$	$\langle\mathcal{O}_1^H[^3P_1]\rangle$ $(\mathcal{O}(\alpha_s^3))$
χ_{c2}	$\langle\mathcal{O}_8^H[^3S_1]\rangle$ $(\mathcal{O}(\alpha_s^2))$	$\langle\mathcal{O}_1^H[^3P_2]\rangle$ $(\mathcal{O}(\alpha_s^2))$	

[a] $\Delta_8^H = \langle\mathcal{O}_8^H[^1S_0]\rangle + \frac{3}{m_c^2}\langle\mathcal{O}_8^H[^3P_0]\rangle + \frac{4}{5m_c^2}\langle\mathcal{O}_8^H[^3P_2]\rangle$.

Table 2
NRQCD LDMEs for the charmonium production in Ref. [24], all in units of GeV^3.

H	$\langle\mathcal{O}_1^H[^3S_1]\rangle$	$\langle\mathcal{O}_1^H[^3P_0]\rangle/{m_c}^2$	$\langle\mathcal{O}_8^H[^3S_1]\rangle$	Δ_8^H
J/ψ	1.16		6.6×10^{-3}	3×10^{-2}
$\psi(2S)$	0.76		4.6×10^{-3}	5.2×10^{-3}
χ_{c0}		0.044	3.2×10^{-3}	

x_1 and x_2. The μ_F and μ_R are the factorization and renormalization scales. The total cross sections are obtained by integrating over x_F.

The production cross section $\hat{\sigma}[ij \to H]$ is the sum of the products of the short-distance coefficients $C^{ij}_{c\bar{c}[n]}$, calculated perturbatively in powers of $\alpha_s(\mu_R)$, and the nonperturbative parameters, LDMEs $\langle\mathcal{O}_n^H[^{2S+1}L_J]\rangle$. The coefficients $C^{ij}_{c\bar{c}[n]}$ describe the production of a $c\bar{c}$ pair in a specific spin-color state $[n]$, while the parameters $\langle\mathcal{O}_n^H[^{2S+1}L_J]\rangle$ account for the hadronization of the $c\bar{c}[n]$ pair into the charmonium state H. The LDMEs are mainly determined by a fit to data and assumed to be universal, independent of beam or target hadrons and the energy scale.

In this work, we use the expressions given in Ref. [24] for computation of J/ψ, $\psi(2S)$, and χ_{cJ} production via GG, $q\bar{q}$ and qG processes. The scattering processes $q\bar{q} \to Q\bar{Q}$ and $GG \to Q\bar{Q}$ at $\mathcal{O}(\alpha_s^2)$ produce $Q\bar{Q}$ pairs in an S-wave CO state or P-wave CS state. Starting from $\mathcal{O}(\alpha_s^3)$, the S-wave or P-wave CS $Q\bar{Q}$ pairs can be produced through the scattering processes $GG \to Q\bar{Q}G$ and $qG \to Q\bar{Q}q$ [26]. We use this NRQCD naframework for calculating the total cross sections of J/ψ and $\psi(2S)$ production in hadronic collision.

The relationship of LDMEs to the scattering processes for each charmonium state is summarized in Table 1. For the $q\bar{q}$ process, the $c\bar{c}$ pairs are produced at $\mathcal{O}(\alpha_s^2)$ in color octet states which then hadronize into various charmonium states with the LDMEs $\langle\mathcal{O}_8^H[^3S_1]\rangle$. For the GG process, both J/ψ, and $\psi(2S)$ can be produced from either the CO $c\bar{c}$ at $\mathcal{O}(\alpha_s^2)$ or the CS $c\bar{c}$ at $\mathcal{O}(\alpha_s^3)$. The corresponding hadronization LDMEs for the CO and CS states are $\Delta_8^H = \langle\mathcal{O}_8^H[^1S_0]\rangle + 3/m_c^2\langle\mathcal{O}_8^H[^3P_0]\rangle + 4/(5m_c^2)\langle\mathcal{O}_8^H[^3P_2]\rangle$ and $\langle\mathcal{O}_1^H[^3S_1]\rangle$, respectively. The χ_{c0}, χ_{c1} and χ_{c2} can be produced from CS $c\bar{c}$ states in the GG process at either $\mathcal{O}(\alpha_s^2)$ (χ_{c0}, χ_{c2}) or $\mathcal{O}(\alpha_s^3)$ (χ_{c1}) with the corresponding hadronization LDMEs $\langle\mathcal{O}_1^H[^3P_0]\rangle/m_c^2$, $\langle\mathcal{O}_1^H[^3P_1]\rangle/m_c^2$ and $\langle\mathcal{O}_1^H[^3P_2]\rangle/m_c^2$. At $\mathcal{O}(\alpha_s^3)$, the qG process can contribute to the production of χ_{c1} via the CS $c\bar{c}$ state, which hadronizes with the LDME $\langle\mathcal{O}_1^H[^3P_1]\rangle/m_c^2$.

The number of independent LDMEs is further reduced by applying the spin symmetry relations [24,27]:

$$\begin{aligned}
\langle\mathcal{O}_8^{J/\psi,\psi(2S)}[^3P_J]\rangle &= (2J+1)\langle\mathcal{O}_8^{J/\psi,\psi(2S)}[^3P_0]\rangle \text{ for } J=2\\
\langle\mathcal{O}_8^{\chi_{cJ}}[^3S_1]\rangle &= (2J+1)\langle\mathcal{O}_8^{\chi_{c0}}[^3S_1]\rangle \text{ for } J=1,2\\
\langle\mathcal{O}_1^{\chi_{cJ}}[^3P_J]\rangle &= (2J+1)\langle\mathcal{O}_1^{\chi_{c0}}[^3P_0]\rangle \text{ for } J=1,2.
\end{aligned} \tag{4}$$

The best-fit LDMEs for the description of proton-induced J/ψ and $\psi(2S)$ production from Ref. [24] are summarized in Table 2. In Ref. [24], the CS LDMEs $\langle\mathcal{O}_1^H[^3S_1]\rangle$ for J/ψ and $\psi(2S)$, and $\langle\mathcal{O}_1^H[^3P_0]\rangle$ for χ_{c0}, are given by the potential models [25], and the CO LDMEs $\langle\mathcal{O}_8^H[^3S_1]\rangle$ for J/ψ, $\psi(2S)$ and χ_c, are taken from the fits to Tevatron collider data of p_T spectra [26]. The Δ_8^H parameters for the individual J/ψ and $\psi(2S)$ production were determined by a fit of NRQCD calculation to the proton-induced data.

A later study by Maltoni et al. [27] was performed with a full NLO calculation [28]. Starting with the LDMEs determined from the collider data of p_T differential cross sections [29,30], an additional reduction factor of about 0.1 for $\langle\mathcal{O}_8^H[^3S_1]\rangle$ and $\langle\mathcal{O}_8^H[^1S_0]\rangle$ of J/ψ and $\psi(2S)$, was required in the calculations to achieve a good description of fixed-target proton-induced data.

The CS LDMEs used in these two studies are either identical or very similar, as they were obtained from a potential model [25]. The CO $\langle\mathcal{O}_8^H[^3S_1]\rangle$ for χ_{c0} are nearly identical. In contrast, the remaining CO LDMEs obtained in Ref. [24] are about a factor of 1.5-5 larger than those determined in Ref. [27].

With the information of LDMEs, the direct production cross sections of J/ψ, $\psi(2S)$ and three χ_{cJ} states can be calculated as shown in Eq. (1). Furthermore, taking into account the direct production of J/ψ and the feed-down from hadronic decays of $\psi(2S)$ and radiative decays of three χ_{cJ} states, the total J/ψ cross section is estimated as follows,

$$\sigma_{J/\psi} = \sigma^{direct}_{J/\psi} + Br(\psi(2S) \to J/\psi X)\sigma_{\psi(2S)} + \sum_{J=0}^{2} Br(\chi_{cJ} \to J/\psi\gamma)\sigma_{\chi_{cJ}} \tag{5}$$

Table 3
The reduced χ^2/ndf of the whole data sets, the χ^2 divided by the number of data point (ndp) for each data set in "Fit-R", "Fit-1" and "Fit-2" NRQCD calculations and the corresponding input or best-fit LDMEs. All LDMEs are in units of GeV^3.

	Fit-R	Fit-1	Fit-2
χ^2_{total}/ndf	16.8	6.0	3.3
$\chi^2/\text{ndp}\vert^p_{\sigma(J/\psi)}$	9.2	4.1	5.4
$\chi^2/\text{ndp}\vert^p_{\sigma(\psi(2S))}$	2.2	1.4	1.7
$\chi^2/\text{ndp}\vert^p_{R(\psi(2S))}$	1.1	0.7	1.0
$\chi^2/\text{ndp}\vert^{\pi^-}_{\sigma(J/\psi)}$	46.8	15.3	3.7
$\chi^2/\text{ndp}\vert^{\pi^-}_{\sigma(\psi(2S))}$	2.8	0.9	0.7
$\langle\mathcal{O}_8^{J/\psi}[^3S_1]\rangle$	6.6×10^{-3}	$(1.47\pm0.07)\times10^{-1}$	$(9.5\pm0.4)\times10^{-2}$
$\Delta_8^{J/\psi}$	3×10^{-2}	$(0\pm8)\times10^{-4}$	$(1.8\pm0.2)\times10^{-2}$
$\langle\mathcal{O}_8^{\psi(2S)}[^3S_1]\rangle$	4.6×10^{-3}	$(2.5\pm0.2)\times10^{-2}$	$(2.6\pm0.2)\times10^{-2}$
$\Delta_8^{\psi(2S)}$	5.2×10^{-3}	$(0\pm8)\times10^{-4}$	$(4\pm6)\times10^{-4}$

For the branching ratios we take the PDG 2020 values [32]

$$Br(\psi(2S)\to J/\psi X)=61.4\%, \qquad Br(\chi_{c0}\to J/\psi\gamma)=1.4\%$$
$$Br(\chi_{c1}\to J/\psi\gamma)=34.3\%, \qquad Br(\chi_{c2}\to J/\psi\gamma)=19.0\%. \tag{6}$$

Using this NRQCD framework, we calculate below the J/ψ and $\psi(2S)$ production cross sections and compare them to the available fixed-target data. We explore if a set of LDMEs can be identified to achieve a good description of both proton-induced and pion-induced data of charmonia production.

3. Results of NRQCD calculations

In this section, we compare our NRQCD calculations with the fixed-target data of J/ψ and $\psi(2S)$ production by proton and pion beams. The cross sections for proton-induced J/ψ and $\psi(2S)$ and their ratios $R_\psi=\sigma(\psi(2S))/\sigma(J/\psi)$ are taken from Ref. [27]. The pion-induced data for J/ψ and $\psi(2S)$ are taken from Refs. [1,33]. In addition, three measurements of R_ψ from HERA [34] and NA38 [35], and the pion-induced data of $\sigma(J/\psi)$ and $\sigma(\psi(2S))$ from NA38 [36] and WA92 [37] are added.

In spite of a caveat of double counting by including the data of R_ψ in the analysis [27], the cancellation of systematic uncertainties in this quantity brings additional constraining power in the fit. The NRQCD calculations presented in this section are performed using the nucleon CT14nlo PDFs [38] and the pion GRV NLO PDFs [22] under the LHAPDF framework [39,40]. The cross sections are evaluated with a charm quark mass $m_c=1.5$ GeV/c^2 and renormalization and factorization scale $\mu_R=\mu_F=2m_c$ [24].

3.1. Reference fit

We compare these data with the NRQCD calculations using the LDMEs determined in Ref. [24], named as "Fit-R" in the following. The difference between the proton PDFs selected for the study of Ref. [24] (CTEQ3L) and here (CT14nlo) has a negligible effect on the final results. The results are plotted as black dashed lines in Fig. 1. The total reduced χ^2/ndf, together with the deviations between data and calculations per data point (χ^2/ndp) for each data set, are displayed in Fig. 1 and listed in Table 3. The reduced χ^2/ndf of the entire data sets is 16.8. Clearly, the pion-induced data below $\sqrt{s}=20$ GeV are significantly underestimated by the calculations as already observed in Ref. [24].

3.2. Fit of the proton-induced data

It is known that the $q\bar{q}$ contribution plays an important role in the pion-induced J/ψ production near threshold because the parton density at large x is dominated by the valence antiquarks in pions [19]. In our NRQCD framework, the $\langle\mathcal{O}_8^H[^3S_1]\rangle$ LDMEs are responsible for the $q\bar{q}$ contribution, as shown in Table 1, and their values were taken from the fits to the Tevatron data [26] at high energies. The observed underestimation of low-energy pion-induced data in "Fit-R" could arise from too small a value for the input $\langle\mathcal{O}_8^H[^3S_1]\rangle$.

To seek an improved description of the pion-induced data, we take a different approach, called "Fit-1", of leaving both $\langle\mathcal{O}_8^H[^3S_1]\rangle$ and Δ_8^H LDMEs for J/ψ and $\psi(2S)$ as free parameters in the global fit of the proton-induced data. The CO LDME of χ_{c0} is fixed at the value given in Ref. [24] and the best-fit LDMEs are required to be positive-definite. The resulting fit is shown as blue dot-dashed lines in Fig. 1. The cross sections for both proton- and pion-induced data are significantly enhanced, compared to the results of "Fit-R". The agreement between the data and calculation is greatly improved. As shown in Table 3, the overall χ^2/ndf is reduced from 16.8 to 6.0, compared to "Fit-R". While the pion-induced data are not used in the global fit for the LDMEs determination, these data are included in the evaluation of χ^2/ndf for comparison purposes.

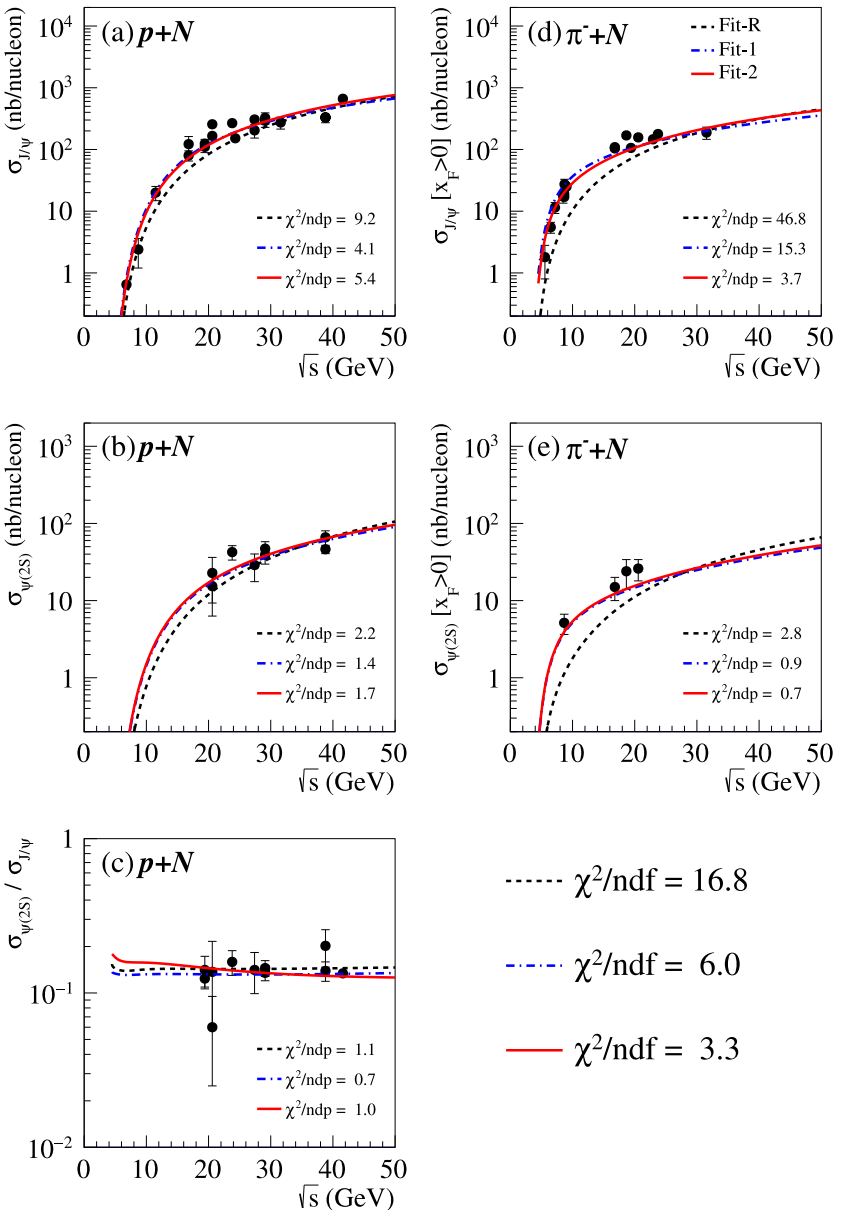

Fig. 1. J/ψ and $\psi(2S)$ production cross sections and the $\psi(2S)/(J/\psi)$ ratios in the $p+N$ reactions, and J/ψ and $\psi(2S)$ production cross sections in the $\pi^- + N$ reactions, labeled as (a)–(e) in the plot. The dashed (black), dot-dashed (blue) and solid (red) curves represent the NRQCD results using the LDMEs obtained in "Fit-R", "Fit-1" and "Fit-2", respectively. The reduced χ^2/ndf for all data are displayed in the bottom-right. The values of χ^2 divided by the number of data point (ndp) for each data set are also shown.

More specifically, the agreement between the pion-induced J/ψ data alone and the calculations with best-fit LDMEs of "Fit-1" is improved by a factor of 3, compared to "Fit-R". The values of newly determined $\langle \mathcal{O}_8^H[^3S_1] \rangle$ LDMEs are 1.5×10^{-1} and 2.5×10^{-2} for J/ψ and $\psi(2S)$, respectively. Both are significantly larger than the "Fit-R" values of 6.6×10^{-3} and 4.6×10^{-3} determined from collider data. The increase of the values of $\langle \mathcal{O}_8^H[^3S_1] \rangle$ clearly accounts for the better agreement between the NRQCD calculations and the pion-induced data, even though the pion data were not included in the fit.

The values of the CO Δ_8^H LDMEs for J/ψ and $\psi(2S)$ resulting from "Fit-1" are compatible with zero, as shown in Table 3. Despite an improved description of data in this approach, "Fit-1" finds vanishing values of Δ_8^H for both J/ψ and $\psi(2S)$. It appears that these LDMEs cannot be determined from the proton-induced J/ψ and $\psi(2S)$ production data alone. This suggests the need to include also the pion data in the global fit, as discussed next.

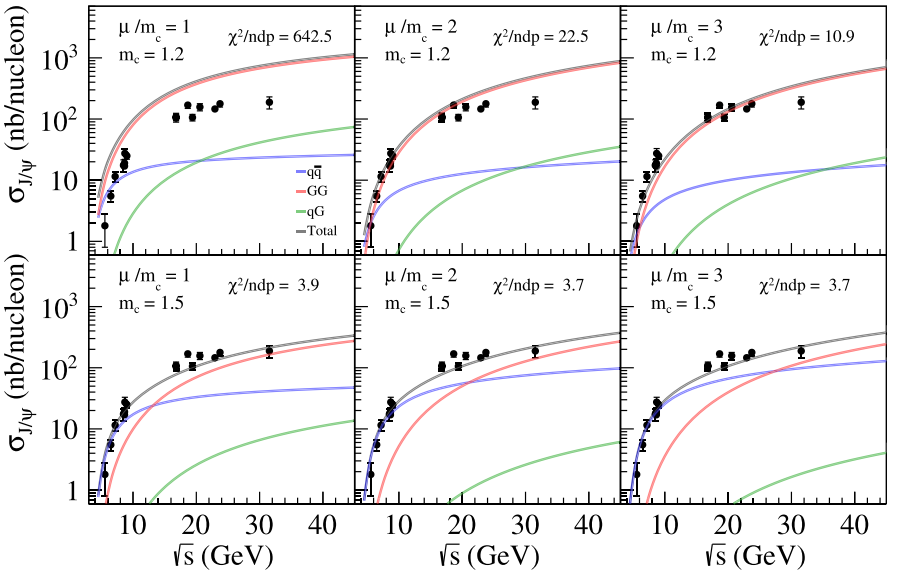

Fig. 2. The NRQCD results from an analysis of both proton-induced and pion-induced data sets under variation of charm quark mass m_c, renormalization scale μ_R and factorization scale μ_F, compared with the pion-induced data of J/ψ production as a function of $\sqrt{s}$. The total cross sections and $q\bar{q}$, GG, and qG contributions are denoted as black, blue, red and green lines, respectively. The values of m_c, $\mu = \mu_R = \mu_F$ in the NRQCD calculation as well as the best-fit χ^2/ndp are displayed in each plot. (For interpretation of the references to color in this figure legend, the reader is referred to the web version of this article.)

3.3. Fit of both the pion- and proton-induced data

Because of the different nature of valence quarks in the protons and pions, the energy dependence of the relative contributions of $q\bar{q}$ and GG processes is different for the J/ψ and $\psi(2S)$ production, especially at low energies. Under the assumption that higher-twist effects are negligible, a combined fit of these two data sets should further constrain the CO LDMEs. The results of this new fit, referred to as "Fit-2", are shown in Table 3 and displayed as the solid red lines in Fig. 1.

Comparing the results of "Fit-2" and "Fit-1", it is found that the description of the pion-induced data is improved, while maintaining a good agreement between the proton data and the calculation. The CO matrix elements are also better constrained. The total reduced χ^2/ndf is further decreased to about 3.3. The agreement between the pion-induced J/ψ data and the NRQCD calculation is improved by a factor of 4, from a χ^2/ndp of 15.3 in "Fit-1" to 3.7 in "Fit-2". The values of the newly determined CO $\langle \mathcal{O}_8^H[^3S_1] \rangle$ LDMEs are 9.5×10^{-2} and 2.6×10^{-2} for J/ψ and $\psi(2S)$, respectively, either smaller than or consistent with those obtained in "Fit-1".

With the inclusion of the pion-induced data, non-zero values of the CO Δ_8^H LDMEs can now be obtained. As shown in Table 3, the values of CO Δ_8^H LDMEs are found to be 1.8×10^{-2} and 4.0×10^{-4} for J/ψ and $\psi(2S)$, respectively. The best-fit $\langle \mathcal{O}_8^H[^3S_1] \rangle$ LDMEs responsible for the contribution of the $q\bar{q}$ process are larger by about a factor of 10, while the Δ_8^H related to the contribution of the GG process are reduced by a factor of 2–10, in comparison with the LDMEs determined from collider data [26,29]. The new CO LDMEs indicate that the $q\bar{q}$ contribution determined by the fixed-target data is significantly larger than the corresponding contribution at collider energies.

The systematic uncertainties of these results are studied by setting m_c to 1.2 GeV/c^2 or 1.5 GeV/c^2 and the normalization scale $\mu = \mu_R = \mu_R$ to m_c, $2m_c$, and $3m_c$. Fig. 2 shows the comparison of the pion-induced J/ψ data and NRQCD calculation with the corresponding settings of m_c and μ. The total cross sections and the $q\bar{q}$, GG, and qG contributions are denoted as black, blue, red and green lines, respectively.

The parameter of the charm quark mass m_c plays a significant role in the systematic effect. With m_c set to 1.2 GeV/c^2, the CO LDMEs as free parameters are not well constrained, and the quality of fit significantly deteriorates as seen from the increased χ^2/ndp. Judging from the contributions of various subprocesses, the GG process is enhanced too much to provide a good description of data in the calculations with this reduction of m_c. When m_c is set as 1.5 GeV/c^2, the quality of the fit is equally good with μ varying among m_c, $2m_c$, and $3m_c$. Even though one of CO LDMEs cannot be obtained with good accuracy when μ is set at m_c, the best-fit LDMEs for three different scales are consistent with having large values of $\langle \mathcal{O}_8^H[^3S_1] \rangle$ LDMEs, reflecting a non-negligible $q\bar{q}$ contribution.

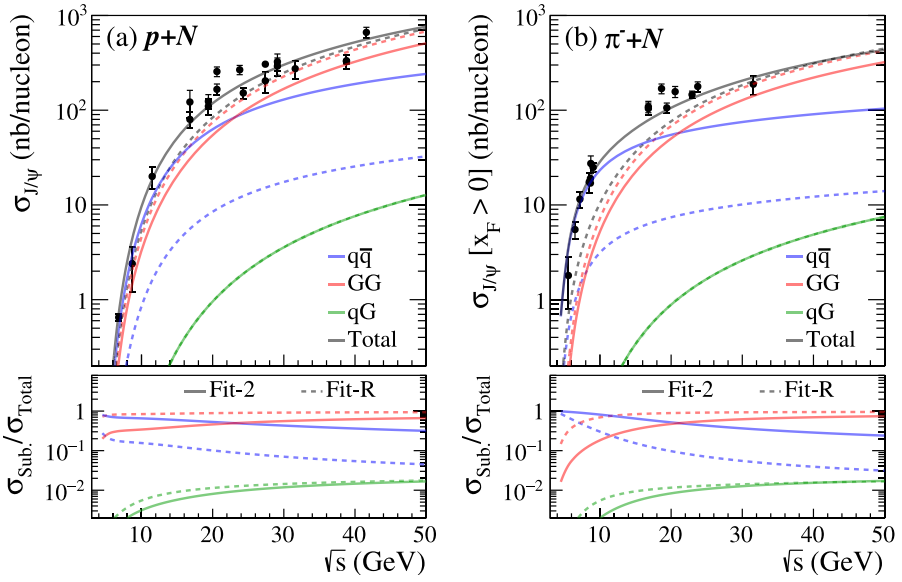

Fig. 3. Total cross sections (black) and contributions from $q\bar{q}$ (blue), GG (red) and qG (green) processes for J/ψ production as a function of $\sqrt{s}$ in (a) pN and (b) $\pi^- N$ interactions. The dashed and solid curves represent the "Fit-R" and "Fit-2" results. The fractions of each sub-process cross section are displayed at the bottom of each plot. (For interpretation of the references to color in this figure legend, the reader is referred to the web version of this article.)

4. Discussion

4.1. Fractions of individual contributions in hadroproduction

A new set of LDMEs for J/ψ and $\psi(2S)$ production at fixed-target energies has been obtained in an analysis of data with proton and pion beams. Our analysis differs from that of Ref. [24] in two aspects. First, the LDMEs $\langle \mathcal{O}_8^H[^3S_1]\rangle$ are now allowed to vary in the global fit. This leads to a much improved description of fixed-target data with proton beam. Second, the pion data are included in the global fit. This allows for the determination of the LDMEs Δ_8^H.

To better understand the reasons for the significantly improved description of the J/ψ and $\psi(2S)$ production data, it is instructive to compare the NRQCD calculations using the "Fit-R" LDMEs of Ref. [24] and the "Fit-2" LDMEs of the present analysis. In particular, we examine the decomposition of the J/ψ production cross section into individual contributions in three fashions: (i) $q\bar{q}$, GG, and qG subprocesses; (ii) color singlet versus color octet $c\bar{c}$ states; (iii) direct production of J/ψ versus feed-down from $\psi(2S)$ and χ_c.

The decomposition of J/ψ production cross sections for proton and pion beams into the $q\bar{q}$, GG and qG processes is shown in Fig. 3. We note that the qG contributions remain unchanged in the new analysis since the qG process only contributes to the formation of the χ_{c1} states and the LDMEs for χ_{cJ} are identical for "Fit-R" and "Fit-2". Fig. 3 also shows that the GG contribution is dominant in the J/ψ production with proton beam at all energies, except near the threshold. In contrast, the $q\bar{q}$ contribution for pion-induced data is enhanced due to the increased antiquark content in pion's valence region. Therefore, the inclusion of the pion data in the global fit provides additional constraints on those LDMEs which are sensitive to the $q\bar{q}$ process. The low-energy fixed-target pion data are particularly important for the determination of the $\langle \mathcal{O}_8^H[^3S_1]\rangle$ LDMEs.

In comparison with "Fit-R", the $\langle \mathcal{O}_8^H[^3S_1]\rangle$ LDME is increased, whereas Δ_8^H is decreased. These changes lead to an enhancement of the CO $q\bar{q}$ contribution and a reduction of the CO GG contribution. The increase of the fraction of $q\bar{q}$ contribution, especially at low-energies, accounts for the improvement in describing the pion data. The opposite trend in the variations of the two CO LDMEs $\langle \mathcal{O}_8^H[^3S_1]\rangle$ and Δ_8^H leads to significant changes in the energy dependence of J/ψ production cross sections, as shown in Fig. 3.

Fig. 4 shows the decomposition of the J/ψ cross sections into contributions from the color octet and color singlet states. As the CS contribution (blue lines) in our study is fixed, the enlarged $\langle \mathcal{O}_8^H[^3S_1]\rangle$ LDMEs significantly enhance the CO contribution (red lines) at low energies, while in "Fit-2" the reduced Δ_8^H results in a reduction of the CO contribution at high energies. Through the interplay of these two CO LDMEs and the parton luminosities, the CO contribution remains similar at high energies but is enhanced near threshold for the proton-induced production. In the case of pion-induced production, the CO contribution is slightly suppressed at high energies.

Fig. 5 shows the decomposition of the J/ψ cross sections into the contributions from direct production (red lines) and the feed-down from heavier charmonium states of $\psi(2S)$ (blue lines) and χ_c (green lines). We note that the LDMEs for the three χ_c states are kept unchanged for "Fit-R" and "Fit-2". The most notable change between the calculations with "Fit-2" and the "Fit-R" is the enhancement of the direct J/ψ production at low energies, as a consequence of an enlarged $\langle \mathcal{O}_8^H[^3S_1]\rangle$. Taking into account

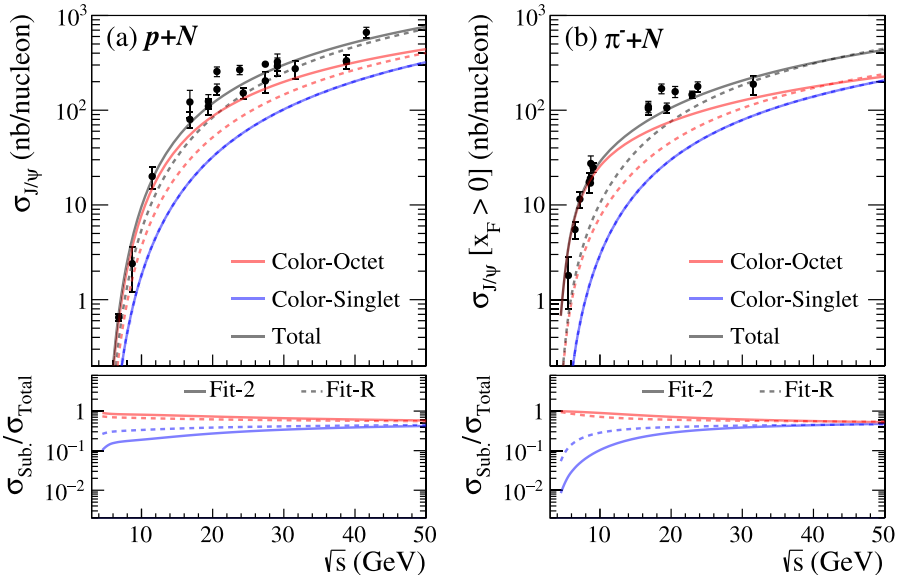

Fig. 4. Same as Fig. 3 for the decomposition of contributions from CS (blue) and CO (red) processes.

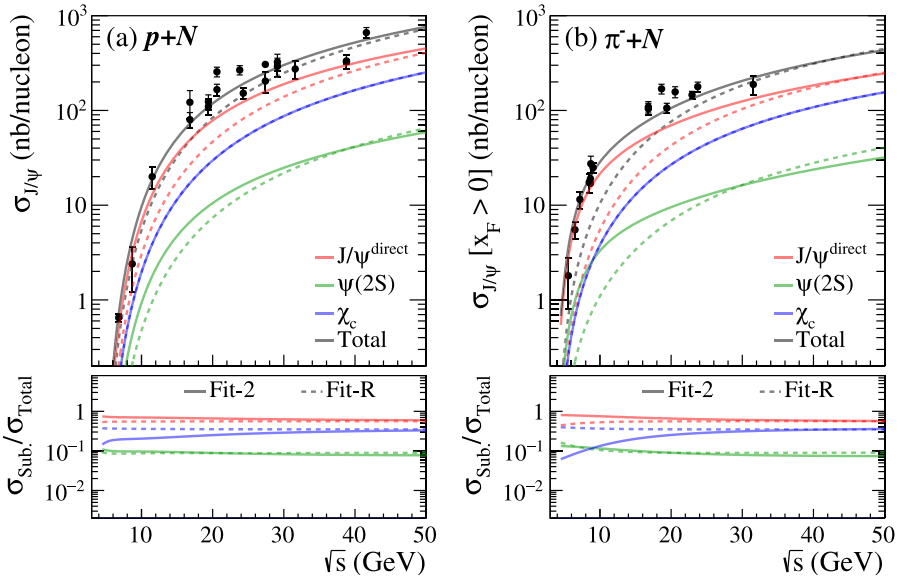

Fig. 5. Same as Fig. 3 for the decomposition of contributions of J/ψ production from direct production of J/ψ (red) and feed-down from $\psi(2S)$ (green) and all χ_c states (blue).

the decay branching ratios, the contributions to the J/ψ production in descending order of importance are direct production, χ_c, and $\psi(2S)$.

To recapitulate the main findings at this point, we note that the inclusion of the low-energy pion-induced total cross section data of J/ψ and $\psi(2S)$ production to the analysis of NRQCD provides an important constraint of the $\langle \mathcal{O}_8^H[^3S_1] \rangle$ LDMEs via the $q\bar{q}$ contributions. A good description of both proton- and pion-induced data by NRQCD can be achieved. The $q\bar{q}$ and CO contributions from the NRQCD calculations with the new LDMEs are greatly enhanced at low energies with proton and pion beams, compared with results found in the earlier studies [24,27].

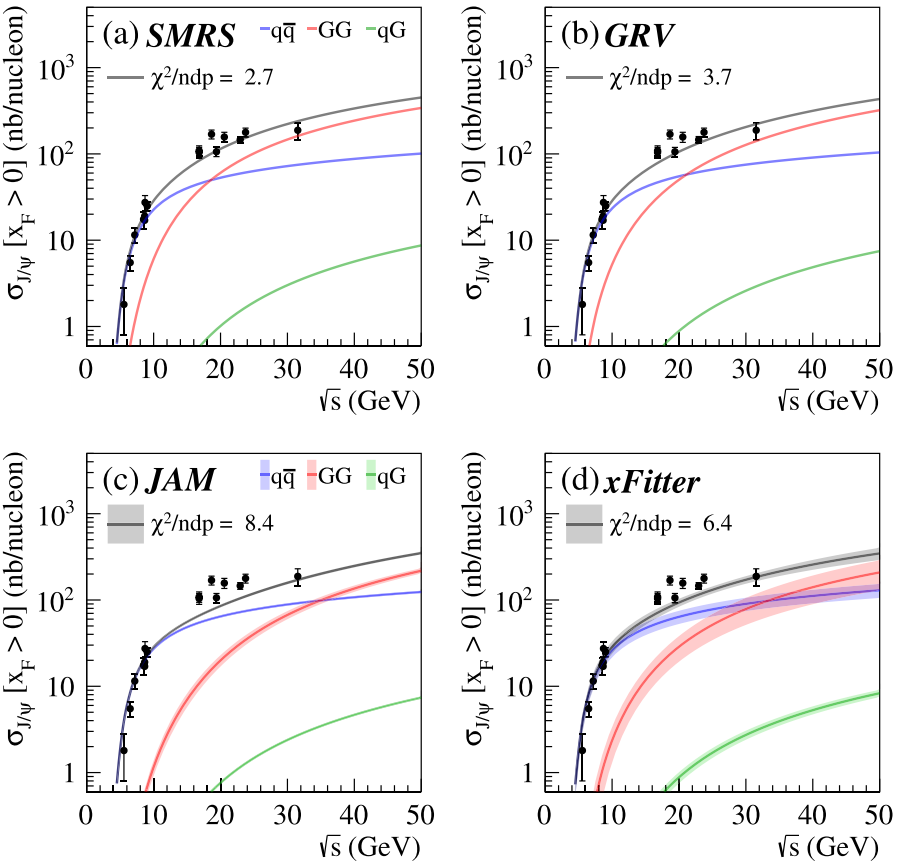

Fig. 6. The NRQCD J/ψ production cross sections at $x_F > 0$ for the $\pi^- N$ reactions, calculated for four pion PDFs (SMRS, GRV, JAM and xFitter) using LDMEs of "Fit-2". The black, blue, red, and green curves represent the calculated total cross sections, and the $q\bar{q}$, GG, and qG contributions, respectively. The shaded bands on the xFitter and JAM calculations come from the uncertainties of the corresponding PDF sets. The SMRS and GRV PDFs contain no information on uncertainties. (For interpretation of the references to color in this figure legend, the reader is referred to the web version of this article.)

4.2. Sensitivity to the pion PDFs

The new set of LDMEs is now used to study the sensitivity of the J/ψ data to the various pion PDFs. We have considered four pion PDFs, namely, SMRS [21] and GRV [22], representative of the most widely used pion PDFs thus far, as well as JAM [6] and xFitter [7], obtained from very recent global analyses. For SMRS, we select the default one in which the sea quarks carry 15% of the pion momentum at Q^2= 4 GeV^2. As illustrated in Ref. [19], SMRS, JAM, and xFitter have similar valence-quark distributions, while the magnitude of the GRV distribution is smaller by about 20%–30%. For the gluon distributions, SMRS and GRV have similar shapes and magnitudes, while xFitter and JAM have significantly smaller magnitudes by a factor of 2–4.

The NRQCD calculation with each of the four pion PDFs is compared with the data in Fig. 6. Overall, the total cross sections (black lines) for the four pion PDFs exhibit similar $\sqrt{s}$ dependencies. However, the individual terms differ strongly. The $q\bar{q}$ contribution dominates near thresholds and the GG contribution increases rapidly at higher energies, while the qG component is relatively negligible over the whole energy range. The relative fractions of $q\bar{q}$ and GG contributions as a function of $\sqrt{s}$ vary for each pion PDFs, reflecting the differences among their parton distributions. For SMRS and GRV the GG contribution starts to dominate the cross section around $\sqrt{s}$ = 20 GeV. For xFitter and JAM the corresponding values are larger at $\sim\sqrt{s}$ = 35 GeV because of their relatively reduced gluon strength in the valence region.

Table 4 lists the χ^2 values of NRQCD calculations for various data sets and best-fit CO LDMEs for each pion PDF. We find that the χ^2 of the pion-induced J/ψ data strongly correlates with the gluon density of pions over the valence quark regions [19]. The GG contributions are similar for GRV and SMRS, while those for xFitter and JAM are 50%–80% smaller due to their weaker gluon strength at $x = 0.1 - 0.6$, relative to GRV and SMRS [19]. The deficiency of xFitter and JAM in the GG contribution leads to an underestimation of the NRQCD calculations against the data over $\sqrt{s} = 15 - 25$ GeV, as shown in Fig. 6.

Table 4 shows that the dependence of the best-fit LDMEs for J/ψ and $\psi(2S)$ to the pion PDFs is rather mild. We also checked that the overall reduced χ^2/ndf of data for each pion PDF has a very small variation when the calculations are done with the best-fit LDMEs obtained using a different set of pion PDFs.

Table 4
The χ^2 values for the entire data sets and the individual J/ψ and $\psi(2S)$ data set from the NRQCD calculations. The best-fit LDMEs for each pion PDF are in units of GeV^3.

	SMRS	GRV	JAM	xFitter
χ^2_{total}/ndf	3.1	3.4	4.8	4.3
χ^2/ndp$\vert^{\pi^-}_{\sigma(J/\psi)}$	2.7	3.7	8.4	6.4
χ^2/ndp$\vert^{\pi^-}_{\sigma(\psi(2S))}$	0.4	0.7	0.4	0.2
$\langle \mathcal{O}_8^{J/\psi}[^3S_1]\rangle$	$(6.9 \pm 0.3) \times 10^{-2}$	$(9.5 \pm 0.4) \times 10^{-2}$	$(8.3 \pm 0.3) \times 10^{-2}$	$(7.4 \pm 0.9) \times 10^{-2}$
$\Delta_8^{J/\psi}$	$(2.5 \pm 0.2) \times 10^{-2}$	$(1.8 \pm 0.2) \times 10^{-2}$	$(2.0 \pm 0.2) \times 10^{-2}$	$(2.2 \pm 0.2) \times 10^{-2}$
$\langle \mathcal{O}_8^{\psi(2S)}[^3S_1]\rangle$	$(2.1 \pm 0.4) \times 10^{-2}$	$(2.6 \pm 0.2) \times 10^{-2}$	$(2.6 \pm 0.1) \times 10^{-2}$	$(2.3 \pm 0.4) \times 10^{-2}$
$\Delta_8^{\psi(2S)}$	$(1.7 \pm 1.0) \times 10^{-3}$	$(4.0 \pm 6.2) \times 10^{-4}$	$(3.7 \pm 3.4) \times 10^{-4}$	$(0.9 \pm 6.0) \times 10^{-3}$

5. Summary

We have analyzed J/ψ and $\psi(2S)$ hadroproduction data in fixed-target experiments within the framework of NRQCD. The previously reported difficulty [24] of obtaining a consistent description of proton and pion data by NRQCD, is resolved by allowing the CO LDMEs for J/ψ and $\psi(2S)$ to be determined by a simultaneous fit to both proton- and pion-induced data. The pion-induced data, especially at low energies, have a sizeable $q\bar{q}$ contribution and thus provide a strong constraint on the $\langle \mathcal{O}_8^H[^3S_1]\rangle$ LDMEs. This sensitivity is much reduced if the analysis is restricted to the proton-induced data alone. Consequently, the best-fit $\langle \mathcal{O}_8^H[^3S_1]\rangle$ values for both J/ψ and $\psi(2S)$ are found to be about ~10 times larger than that same values obtained using the collider data. In contrast, the best-fit values for Δ_8^H, partly responsible for the GG contribution, are compatible for J/ψ but more than 10 times smaller for $\psi(2S)$, compared to the results of Ref. [24].

The resulting LDMEs combined with four different pion PDFs were used to compare the NRQCD calculation with the pion-induced J/ψ production cross-sections. The pronounced differences between the predicted individual quark–antiquark annihilation and gluon–gluon fusion terms result from the different shapes and magnitudes of the corresponding PDF parametrizations. When compared to the total cross section, the SMRS or GRV PDFs still provide a slightly better description of the data than JAM or xFitter, suggesting that the data favor those PDFs with larger gluon contents at medium and large x. All these results are in line with our earlier findings [19] obtained with the CEM.

We note that there are the recent state-of-the-art NLO NRQCD fits [41–44] to collider data. The $\langle \mathcal{O}_8^{J/\psi}[^3S_1]\rangle$ LDMEs found in Refs. [41,43] are substantially smaller than our results. In the fixed-target domain considered here the mean p_T values are lower than the charmonium mass. In this low-p_T region the factorization assumption of NRQCD may no longer be valid. Higher-order corrections or other additional contributions could therefore spoil the universality of the LDMEs. It will be interesting to perform similar studies, including the pion-induced data of charmonium production with the full NLO NRQCD formalism and make a comparison with the current results in the future.

In the near future, new measurements of Drell–Yan as well as J/ψ data in $\pi^- N$ reactions will be available from the CERN COMPASS [45] and AMBER [46] experiments. While future theoretical advances are needed to further reduce the model dependence in describing the J/ψ production, we emphasize the importance of including the pion-induced J/ψ data in future pion PDF global analysis.

Declaration of competing interest

The authors declare that they have no known competing financial interests or personal relationships that could have appeared to influence the work reported in this paper.

Acknowledgments

We thank Nobuo Sato and Ivan Novikov for providing us with LHAPDF6-compatible grid files of JAM and xFitter PDFs. This work was supported in part by the U.S. National Science Foundation (Grant PHY18-22502) and the Ministry of Science and Technology of Taiwan.

References

[1] G.A. Schuler, Quarkonium production and decays, arXiv:hep-ph/9403387.
[2] G.A. Schuler, Production of heavy quarks and heavy quarkonia, Z. Phys. C 71 (1996) 317.
[3] N. Brambilla, et al., Heavy quarkonium: Progress, puzzles, and opportunities, Eur. Phys. J. C 71 (2011) 1534.
[4] A. Andronic, et al., Heavy-flavour and quarkonium production in the LHC era: from proton–proton to heavy-ion collisions, Eur. Phys. J. C 76 (2016) 107.
[5] J.P. Lansberg, New observables in inclusive production of quarkonia, Phys. Rep. 889 (2020) 1.
[6] P.C. Barry, N. Sato, W. Melnitchouk, C.R. Ji, First Monte Carlo global QCD analysis of pion parton distributions, Phys. Rev. Lett. 121 (2018) 152001.
[7] I. Novikov, et al., Parton distribution functions of the charged pion within the xfitter framework, Phys. Rev. D 102 (2020) 014040.
[8] C. Bourrely, F. Buccella, J.C. Peng, A new extraction of pion parton distributions in the statistical model, Phys. Lett. B 813 (2021) 136021.

[9] K.D. Bednar, I.C. Cloët, P.C. Tandy, Distinguishing quarks and gluons in pion and kaon PDFs, Phys. Rev. Lett. 124 (2020) 042002.
[10] Z.F. Cui, et al., Kaon and pion parton distributions, Eur. Phys. J. C 80 (2020) 1064.
[11] G.F. de Teramond, et al., [HLFHS Collaboration], Universality of generalized parton distributions in light-front holographic QCD, Phys. Rev. Lett. 120 (2018) 182001.
[12] J. Lan, C. Mondal, S. Jia, X. Zhao, J.P. Vary, Parton distribution functions from a light front hamiltonian and QCD evolution for light mesons, Phys. Rev. Lett. 122 (2019) 172001.
[13] J.H. Zhang, J.W. Chen, L. Jin, H.W. Lin, A. Schäfer, Y. Zhao, First direct lattice-QCD calculation of the x-dependence of the pion parton disution function, Phys. Rev. D 100 (2019) 034505.
[14] R.S. Sufian, J. Karpie, C. Egerer, K. Orginos, J.W. Qiu, D.G. Richards, Pion valence quark distribution from matrix element calculated in lattice QCD, Phys. Rev. D 99 (2019) 074507.
[15] T. Izubuchi, L. Jin, C. Kallidonis, N. Karthik, S. Mukherjee, P. Petreczky, C. Shugert, S. Syritsyn, Valence parton distribution function of pion from fine lattice, Phys. Rev. D 100 (2019) 034516.
[16] B. Joó, J. Karpie, K. Orginos, A.V. Radyushkin, D.G. Richards, R.S. Sufian, S. Zafeiropoulos, Pion valence structure from ioffe-time parton pseudodistribution functions, Phys. Rev. D 100 (2019) 114512.
[17] R.S. Sufian, et al., Pion valence quark distribution from current-current correlation in lattice QCD, Phys. Rev. D 102 (2020) 054508.
[18] X. Gao, et al., Valence parton distribution of the pion from lattice QCD: Approaching the continuum limit, Phys. Rev. D 102 (2020) 094513.
[19] W.C. Chang, J.C. Peng, S. Platchkov, T. Sawada, Constraining gluon density of pions at large x by pion-induced J/ψ production, Phys. Rev. D 102 (2020) 054024.
[20] M.B. Einhorn, S.D. Ellis, Hadronic production of the new resonances: Probing gluon distributions, Phys. Rev. D 12 (1975) 2007;
H. Fritzsch, Producing heavy quark flavors in hadronic collisions: a test of quantum chromodynamics, Phys. Lett. 67B (1977) 217;
F. Halzen, Cvc for gluons and hadroproduction of quark flavors, Phys. Lett. 69B (1977) 105.
[21] P.J. Sutton, A.D. Martin, R.G. Roberts, W.J. Stirling, Parton distributions for the pion extracted from drell–yan and prompt photon experiments, Phys. Rev. D 45 (1992) 2349.
[22] M. Gluck, E. Reya, A. Vogt, Pionic parton distributions, Z. Phys. C 53 (1992) 651.
[23] G.T. Bodwin, E. Braaten, G.P. Lepage, Rigorous QCD analysis of inclusive annihilation and production of heavy quarkonium, Phys. Rev. D 51 (1995) 1125, 55 (1997) 5853(E).
[24] M. Beneke, I.Z. Rothstein, Hadroproduction of quarkonia in fixed target experiments, Phys. Rev. D 54 (1996) 2005, 54 (1996) 7082(E).
[25] E.J. Eichten, C. Quigg, Quarkonium wave functions at the origin, Phys. Rev. D 52 (1995) 1726.
[26] P.L. Cho, A.K. Leibovich, Color octet quarkonia production, ii, Phys. Rev. D 53 (1996) 6203.
[27] F. Maltoni, et al., Analysis of charmonium production at fixed-target experiments in the NRQCD approach, Phys. Lett. B 638 (2006) 202.
[28] A. Petrelli, M. Cacciari, M. Greco, F. Maltoni, M.L. Mangano, NLO Production and decay of quarkonium, Nuclear Phys. B 514 (1998) 245.
[29] M. Beneke, M. Krämer, Direct J/ψ and ψ' polarization and cross-sections at the fermilab tevatron, Phys. Rev. D 55 (1997) 5269(R).
[30] P. Nason, et al., Bottom production, 1999 Workshop on Standard model physics (and more) at the LHC, 231-304, arXiv:hep-ph/0003142.
[31] R. Vogt, The x(f) dependence of ψ and drell–yan production, Phys. Rev. C 61 (2000) 035203.
[32] P.A. Zyla, et al., (Particle Data Group), Prog. Theor. Exp. Phys. 2020 (2020) 083C01.
[33] R. Vogt, J/ψ Production and suppression, Phys. Rep. 310 (1999) 197.
[34] I. Abt, et al., [HERA-B Collaboration], A measurement of the ψ' to J/ψ production ratio in 920-gev proton-nleus interactions, Eur. Phys. J. C 49 (2007) 545.
[35] C. Baglin, et al., [NA38 Collaboration], Psi-prime and J/ψ production in p w, p u and s u interactions at 200-gev/nucleon, Phys. Lett. B 345 (1995) 617.
[36] M.J. Corden, et al., Experimental results on J/ψ production by $\pi^{\pm}$, $K^{\pm}$, p and $\bar{p}$ beams at 39.5-gev, Phys. Lett. 96B (1980) 411.
[37] Y. Alexandrov, et al., [BEATRICE Collaboration], Inclusive J/ψ and ψ' production in π^{-}-nucleus interactions at $s^{1/2}$ approximately equals 26-gev, Nuclear Phys. B 557 (1999) 3.
[38] S. Dulat, et al., New parton distribution functions from a global analysis of quantum chromodynamics, Phys. Rev. D 93 (2016) 033006.
[39] M.R. Whalley, D. Bourilkov, R.C. Group, The Les Houches accord PDFs (LHAPDF) and LHAGLUE, arXiv:hep-ph/0508110.
[40] A. Buckley, J. Ferrando, S. Lloyd, K. Nordström, B. Page, M. Rüfenacht, M. Schönherr, G. Watt, LHAPDF6: parton density access in the LHC precision era, Eur. Phys. J. C 75 (2015) 132.
[41] M. Butenschoen, B.A. Kniehl, Reconciling J/ψ production at HERA, RHIC, tevatron, and LHC with NRQCD factorization at next-to-leading order, Phys. Rev. Lett. 106 (2011) 022003.
[42] Y.Q. Ma, K. Wang, K.T. Chao, $J/\psi(\psi')$ Production at the tevatron and LHC at $\mathcal{O}(\alpha^{]]})$ in nonrelativistic QCD, Phys. Rev. Lett. 106 (2011) 042002.
[43] M. Butenschoen, B.A. Kniehl, World data of J/ψ production consolidate NRQCD factorization at NLO, Phys. Rev. D 84 (2011) 051501.
[44] Y.Q. Ma, K. Wang, K.T. Chao, A complete NLO calculation of the J/ψ and ψ' production at hadron colliders, Phys. Rev. D 84 (2011) 114001.
[45] M. Aghasyan, et al., [COMPASS Collaboration], First measurement of transverse-spin-dependent azimuthal asymmetries in the drell-yan process, Phys. Rev. Lett. 119 (2017) 112002;
C.Y. Hsieh, JPS Conf. Proc. 26 (2019) 031003.
[46] B. Adams, et al., Letter of Intent: A New QCD facility at the M2 beam line of the CERN SPS (COMPASS++/AMBER), arXiv:1808.00848.